Enhanced efficiency of thin film solar cells using a shifted dual grating plasmonic structure

Ronen Chriki, Avner Yanai, Joseph Shappir, and Uriel Levy*

Department of Applied Physics, The Benin School Engineering and Computer Science, The Hebrew University of Jeruslaem, Jerusalem 91904, Israel

**ulevy@cc.huji.ac.il*

Abstract: We propose an ultrathin solar cell architecture design which incorporates two periodic layers of metallic and dielectric gratings. Both layers couple the incident light to photonic and plasmonic modes, thus increasing absorption within the cell. The relative position between the two gratings is examined, and is shown to have significant impact on absorption. A lateral shift between the two layers introduces structural asymmetry, and enables coupling of the incident field to optically dark photonic modes. Furthermore, the lateral shift influences mode interactions. Current density enhancement is calculated under AM1.5G solar illumination, and is found to reach a value of 1.86. The structure proposed is optimized and compared to solar cells with a single layer of metallic or dielectric nanostructures.

OCIS codes: (350.6050) Solar energy; (050.2770) Gratings; (310.0310) Thin films; (250.5403) Plasmonics; (310.2790) Guided waves.

References and links

1. O. Morton, "Solar energy: A new day dawning? Silicon valley sunrise," Nature **443**(7107), 19–22 (2006).
2. M. A. Green and S. Pillai, "Harnessing plasmonics for solar cells," Nat. Photonics **6**(3), 130–132 (2012).
3. H. A. Atwater and A. Polman, "Plasmonics for improved photovoltaic devices," Nat. Mater. **9**(3), 205–213 (2010).
4. V. E. Ferry, J. N. Munday, and H. A. Atwater, "Design considerations for plasmonic photovoltaics," Adv. Mater. **22**(43), 4794–4808 (2010).
5. R. A. Pala, J. White, E. Barnard, J. Liu, and M. L. Brongersma, "Design of plasmonic thin film solar cells with broadband absorption enhancement," Adv. Mater. **21**(34), 3504–3509 (2009).
6. Y. A. Akimov and W. S. Koh, "Design of plasmonic nanoparticles for efficient subwavelength light trapping in thin-film solar cells," Plasmonics **6**(1), 155–161 (2011).
7. J. N. Munday and H. A. Atwater, "Large integrated absorption enhancement in plasmonic solar cells by combining metallic gratings and antireflection coatings," Nano Lett. **11**(6), 2195–2201 (2011).
8. J. Grandidier, D. M. Callahan, J. N. Munday, and H. A. Atwater, "Light absorption enhancement in thin-film solar cells using whispering gallery modes in dielectric nanospheres," Adv. Mater. **23**(10), 1272–1276 (2011).
9. J. Bhattacharya, N. Chakravarty, S. Pattnaik, W. D. Slafer, R. Biswas, and V. L. Dalal, "A photonic-plasmonic structure for enhancing light absorption in thin film solar cells," Appl. Phys. Lett. **99**(13), 131114 (2011).
10. H. R. Stuart and D. G. Hall, "Absorption enhancement in silicon on insulator waveguides using metal island films," Appl. Phys. Lett. **69**(16), 2327–2329 (1996).
11. H. R. Stuart and D. G. Hall, "Island effects in nanoparticle enhanced photodetectors," Appl. Phys. Lett. **73**(26), 3815–3817 (1998).
12. D. Derkacs, W. V. Chen, P. M. Matheu, S. H. Lim, P. K. L. Yu, and E. T. Yu, "Nanoparticle induced light scattering for improved performance of quantum well solar cells," Appl. Phys. Lett. **93**(9), 091107 (2008).
13. F. J. Beck, S. Mokkapati, A. Polman, and K. R. Catchpole, "Asymmetry in photocurrent enhancement by plasmonic nanoparticle arrays located on the front or on the rear of solar cells," Appl. Phys. Lett. **96**(3), 033113 (2010).
14. V. E. Ferry, L. A. Sweatlock, D. Pacifici, and H. A. Atwater, "Plasmonic nanostructure design for efficient light coupling into solar cells," Nano Lett. **8**(12), 4391–4397 (2008).
15. D. Duche, P. Torchio, L. Escoubas, F. Monestier, J. J. Simon, F. Flory, and G. Mathian, "Improving light absorption in organic solar cells by plasmonic contribution," Sol. Energy Mater. Sol. Cells **93**(8), 1377–1382 (2009).

#181959 - $15.00 USD Received 18 Dec 2012; revised 13 Feb 2013; accepted 25 Mar 2013; published 9 Apr 2013

16. A. Crescitelli, A. Ricciardi, M. Consales, E. Esposito, C. Granata, V. Galdi, A. Cutolo, and A. Cusano, "Nanostructured metallo-dielectric quasi crystals: towards photonic-plasmonic resonance engineering," Adv. Funct. Mater. **22**(20), 4389–4398 (2012).
17. I. Diukman, L. Tzabari, N. Berkovitch, N. Tessler, and M. Orenstein, "Controlling absorption enhancement in organic photovoltaic cells by patterning Au nano disks within the active layer," Opt. Express **19**(S1 Suppl 1), A64–A71 (2011).
18. C. Hägglund, M. Zäch, G. Petersson, and B. Kasemo, "Electromagnetic coupling of light into a silicon solar cell by nanodisk Plasmons," Appl. Phys. Lett. **92**(5), 053110 (2008).
19. B. le Feber, J. Cesario, H. Zeijlemaker, N. Rotenberg, and L. Kuipers, "Exploiting long-ranged order in quasiperiodic structures for broadband plasmonic excitation," Appl. Phys. Lett. **98**(20), 201108 (2011).
20. V. E. Ferry, M. A. Verschuuren, M. C. Lare, R. E. Schropp, H. A. Atwater, and A. Polman, "Optimized spatial correlations for broadband light trapping nanopatterns in high efficiency ultrathin film a-Si:H solar cells," Nano Lett. **11**(10), 4239–4245 (2011).
21. V. E. Ferry, A. Polman, and H. A. Atwater, "Modeling light trapping in nanostructured solar cells," ACS Nano **5**, 10055–10064 (2011).
22. M. A. Sefunc, A. K. Okyay, and H. V. Demir, "Volumetric plasmonic resonator architecture for thin film solar cells," Appl. Phys. Lett. **98**(9), 093117 (2011).
23. H. Shen and B. Maes, "Combined plasmonic gratings in organic solar cells," Opt. Express **19**(S6 Suppl 6), A1202–A1210 (2011).
24. D. Madzharov, R. Dewan, and D. Knipp, "Influence of front and back grating on light trapping in microcrystalline thin-film silicon solar cells," Opt. Express **19**(S2 Suppl 2), A95–A107 (2011).
25. A. Abass, K. Q. Le, A. Alù, M. Burgelman, and B. Maes, "Dual interface grating for broadband absorption enhancement in thin film solar cells," Phys. Rev. B **85**(11), 115449 (2012).
26. S. Hajimirza and J. Howell, "Inverse optimization of plasmonic and antireflective grating thin film PV cells," J. Phys. Conf. Ser. **369**, 012015 (2012).
27. L. Fu, P. Schau, K. Frenner, W. Osten, T. Weiss, H. Schweizer, and H. Giessen, "Mode coupling and interaction in a plasmonic microcavity with resonant mirrors," Phys. Rev. B **84**(23), 235402 (2011).
28. A. Yanai and U. Levy, "Tunability of reflection and transmission spectra of two periodically corrugated metallic plates, obtained by control of the interactions between plasmonic and photonic modes," J. Opt. Soc. Am. B **27**(8), 1523–1529 (2010).
29. V. Ganapati, O. D. Miller, and E. Yablonovitch, "Spontaneous symmetry breaking in the optimization of subwavelength solar cell textures for light trapping," in *Photovoltaic Specialist Conference*, 38th IEEE, 001572–001576 (IEEE, 2012).
30. V. Liu, M. Povinelli, and S. Fan, "Resonance-enhanced optical forces between coupled photonic crystal slabs," Opt. Express **17**(24), 21897–21909 (2009).
31. A. Christ, O. J. F. Martin, Y. Ekinci, N. A. Gippius, and S. G. Tikhodeev, "Symmetry breaking in a plasmonic metamaterial at optical wavelength," Nano Lett. **8**(8), 2171–2175 (2008).
32. T. Okamoto, J. Simonen, and S. Kawata, "Plasmonic band gaps of structured metallic thin films evaluated for a surface plasmon laser using the coupled-wave approach," Phys. Rev. B **77**(11), 115425 (2008).
33. W. Nakagawa and Y. Fainman, "Tunable optical nanocavity based on modulation of near-field coupling between subwavelength periodic nanostructures," IEEE J. Sel. Top. Quantum Electron. **10**(3), 478–483 (2004).
34. M. G. Moharam, E. B. Grann, D. A. Pommet, and T. K. Gaylord, "Formulation for stable and efficient implementation of the rigorous coupled-wave analysis of binary gratings," J. Opt. Soc. Am. A **12**(5), 1068–1076 (1995).
35. P. Lalanne and G. M. Morris, "Highly improved convergence of the coupled-wave method for TM polarization," J. Opt. Soc. Am. A **13**(4), 779–784 (1996).
36. E. D. Palik, *Handbook of Optical Constants of Solids* (Academic, 1985).
37. M. A. Green and M. J. Keevers, "Optical properties of intrinsic silicon at 300 K," Prog. Photovolt. Res. Appl. **3**(3), 189–192 (1995).
38. A. F. Oskooi, D. Roundy, M. Ibanescu, P. Bermel, J. Joannopoulos, and S. G. Johnson, "MEEP: A flexible free-software package for electromagnetic simulations by the FDTD method," Comput. Phys. Commun. **181**(3), 687–702 (2010).
39. National renewable energy laboratory (NREL), National solar radiation database, 1991–2010 update. *http://rredc.nrel.gov/solar/old_data/nsrdb/1991-2010/*

1. Introduction

In the quest for alternative green energy sources, solar cell technology seems to be a promising candidate, as it can supply virtually unlimited amounts of energy [1]. Although solar cell technology has been around for several decades now, it is still an expensive solution compared with fossil fuel or nuclear technologies. In order to reduce material costs, one would like to produce thin film solar cells. However, thin layers generally result in poor absorbance, and therefore the energetic efficiency of solar cells based on thin film technology is low.

#181959 - $15.00 USD Received 18 Dec 2012; revised 13 Feb 2013; accepted 25 Mar 2013; published 9 Apr 2013

To overcome this deficiency, a significant effort is geared towards the research and the development of thin film solar cells with enhanced absorption, by using advanced light trapping techniques [2–4]. The use of nanoscale metallic or dielectric objects either above [5–13], bellow [4, 13–16] or within [17, 18] solar cells has been found to increase the generated photocurrent both theoretically and experimentally. Periodic [4–9, 14, 15], quasi periodic [16, 19] and random [9–13, 18–20] nanoparticle arrays were shown to provide significant absorbance enhancement, mainly by coupling to photonic guided and/or localized modes within the absorbing substrate. Recently, there has been a growing interest in combining several grating layers [21–26].

Here we propose and study combined grating designs, which include two grating layers (a dual grating design) with a lateral shift between them (see Fig. 1). It is known that the presence of one grating structure in the near vicinity of another yields mode interactions. By changing the lateral position of one grating compared to the other, one can modify the nature of interactions between different modes and by doing so it is possible to improve absorption at specific frequencies [27, 28]. Furthermore, introducing a lateral shift between the two grating layers breaks the symmetry of the structure, and enables coupling of the incident light to dark modes which would otherwise be inaccessible at normal incidence [23, 25, 29–32]. Lateral shift between two closely spaced subwavelength gratings was shown to play a major role in controlling the transmission through such a device [33]. Here, the challenge is even larger, as the absorption enhancement needs to be broad band in order to cope with realistic solar cell applications.

To illustrate our proposed approach we employ a periodic one dimensional grating structure consisting of metallic and dielectric strips (Fig. 1). The computer simulations of the periodic structures presented here are based on the rigorous coupled wave analysis (RCWA), also known as the Fourier modal method, improved by factorization rules [34, 35]. The optical constants used in the simulations were extracted from [36] and [37] for the Silicon and for the Silver and ITO materials, respectively. At the closing point of this paper, we will present a generalization to two dimensional gratings. The simulations of these gratings were accomplished using the finite difference time domain (FDTD) algorithm, using a freely available software package [38].

This paper provides several important contributions. First, we propose and analyze a structure consisting of two gratings (top and bottom). We start by optimizing the properties of each of the gratings and then turn into the optimization of the dual grating structure, and in particular the relative shift between the gratings. This shift gives rise to the interaction of the incident light with the various symmetric and anti symmetric modes supported by the structure. By properly choosing the shift, the coupling to highly absorbing modes becomes feasible. Otherwise, these modes are dark modes, i.e. no light is coupled to these modes and thus they do not contribute to absorption enhancement in the thin film structure. Second, it is the first time that a comprehensive comparison between the cases of single and dual grating structures is provided. This comparison clearly shows that the dual grating structure exhibits a significant improvement in absorption compared with the case of a single grating. Finally, a novel 2-D dual grating structure is proposed, showing further improvement in absorption, leading to enhanced current density.

The paper is structured as follows. Section 2 presents the design and the analysis of the 1D grating structures. It begins by considering two single grating structures, which are then compared with the proposed dual grating cell. The photonic and plasmonic modes of these structures are described, and the effect of the lateral shift in the dual grating structure is discussed. Section 3 then turns to demonstrate our basic design with a 2D grating, showing additional enhancement of absorbance within the solar cell's active layer. Finally, section 4 concludes the paper.

#181959 - $15.00 USD Received 18 Dec 2012; revised 13 Feb 2013; accepted 25 Mar 2013; published 9 Apr 2013

2. 1D grating structures

In our simulations we consider a basic reference cell consisting of an ultrathin (100nm thick) layer of crystalline silicon as the active material layer, deposited on top of an infinitely thick Ag substrate, with a 60 nm thick layer of indium-tin-oxide (ITO) deposited on top of the silicon layer. The back Ag layer serves as a back contact and as a reflector, while the front ITO layer serves as a top contact and also as an antireflective layer. Two gratings are added to the structure: a dielectric si-ITO grating and a Ag-si grating on the top and the bottom side of the silicon layer, respectively. Both gratings are facing inwards (into the silicon layer), as shown in Fig. 1(a). To examine the effect of the dual grating structure, we compare our results to the results obtained with a simpler structures consisting of either a single top grating (Fig. 1(a)), or a single bottom grating (Fig. 1(b)).

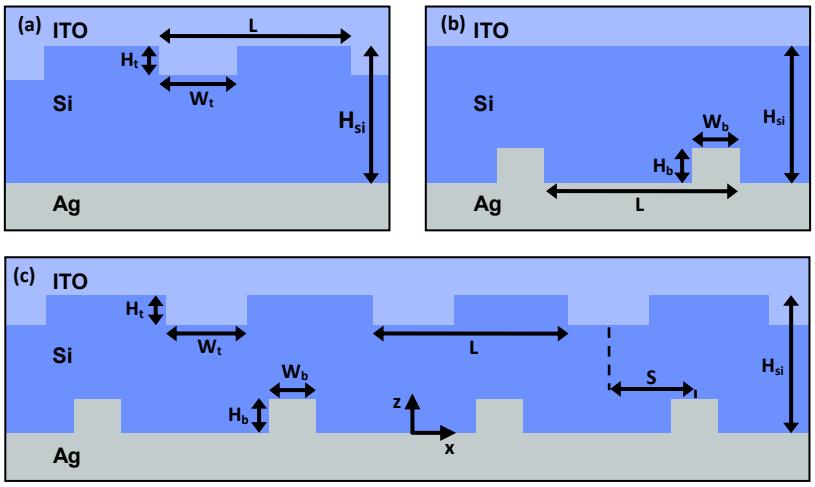

Fig. 1. Schematic diagram of (a) single top grating, (b) single bottom grating, and (c) dual grating solar cells.

2.1 Single grating structures

First we discuss the results obtained with the single grating structures. We optimize the height, width and period of the grating for the purpose of maximizing the short circuit current density J_{SC} as depicted in Fig. 2. J_{SC} is calculated by integrating the wavelength-dependant absorption between 400 and 1100nm, weighted by the AM1.5G solar spectrum function, and by summing the contributions from both TE and TM polarization, accounting for the randomly polarized light emanating from the sun. The resulted current density is normalized to the value obtained for the same cell without the grating structures. Varying the width (W) and height (H) of the top (Fig. 2(a)) and bottom (Fig. 2(b)) gratings, short circuit current enhancement J_{SC} is calculated for a grating period of 425nm. We repeated this process by scanning the grating period in the range of 200-500nm and extracting the maximal value of J_{SC} for each period as a function of W and H. The obtained normalized maximum current density $J_{SC}^{\max}$ is plotted as a function of grating period for the cases of top and bottom grating cells (Figs. 2(c) and 2(d) respectively).

#181959 - $15.00 USD Received 18 Dec 2012; revised 13 Feb 2013; accepted 25 Mar 2013; published 9 Apr 2013

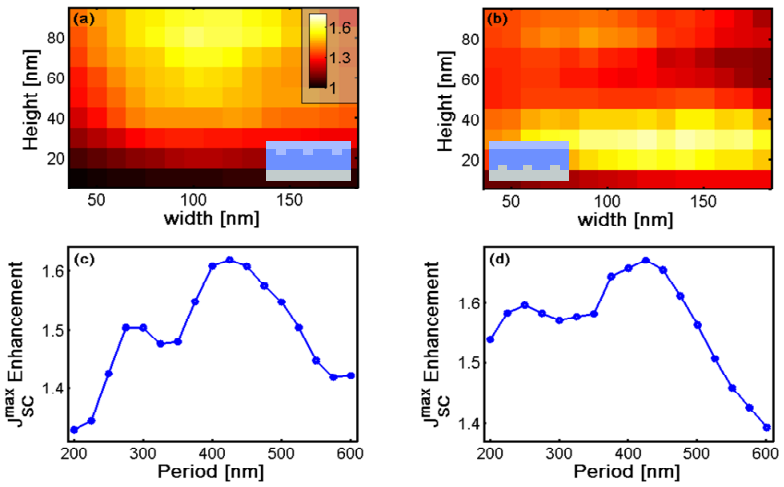

Fig. 2. Optimization procedure of single grating solar cells. Short circuit current density enhancement is shown for single grating structures with periodicity of 425nm, as a function of height and width of the gratings under randomly polarized light at incident angle for (a) top and (b) bottom grating cells. (a) and (b) are illustrated in the same color scale. The optimal width and height are found for each grating period, and the maximal short circuit current density is presented as a function of the period, for (c) top and (d) bottom grating structures.

Figure 3 presents contour plots of absorption enhancement in relation to the same design in the absence of grating structures for TE and TM illuminations as a function of grating wavenumber (2π /period), for the top and bottom single grating cells. These plots show great similarity to the dispersion relations of guided modes. To verify this, dispersion relations of the analytically solved waveguide modes are calculated (energy versus propagation constant β for TE_0, TE_1, TM_0 and TM_1 modes), and the corresponding Bloch modes are plotted (energy versus grating wavenumber K, where $K = \beta / m$ and m being an integer), for a bare ITO-si-Ag structure without dielectric and metallic gratings. As the grating structures intrude the silicon layer, the effective thickness of the silicon layer (H_{si}) is reduced, and the modes are slightly varied. To account for this effect, the analytically solved waveguide modes were calculated for several effective thicknesses in the range of 60-100nm (in steps of 10nm). It was found that the analytically solved modes correlate best with the stronger absorption features of the contour plots for an effective thickness of H_{si} = 80nm for the top and dual grating structures, and for an effective thickness of H_{si} = 90nm for the bottom grating structure. The slight discrepancies are attributed to the presence of the grating structures within the silicon material, which perturb the guided modes.

#181959 - $15.00 USD Received 18 Dec 2012; revised 13 Feb 2013; accepted 25 Mar 2013; published 9 Apr 2013

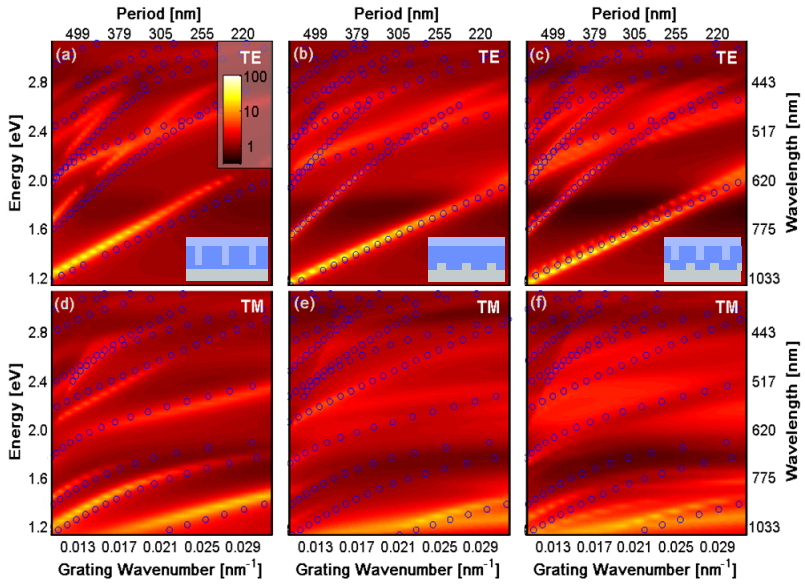

Fig. 3. Absorption enhancement as a function of wavelength and grating wavenumber for (a, d) top, (b, e) bottom and (c, f) dual grating structure, under TE and TM illuminations at incident angle. The bottom grating structure consists of a metallic Ag-Si grating of 30nm height and a duty cycle of 0.282; and the top grating structure consists of a dielectric ITO-Si grating of 80nm height and of a duty cycle of 0.235. The dual grating structure includes both a top and bottom gratings, with the following parameters: 60nm top grating height, 0.188 top grating duty cycle, 30nm bottom grating height, 0.259 bottom grating duty cycle. The circles on the plots correspond to analytically solved propagating waveguide modes, and to their repetitions at higher orders. (a-f) appear in the same color scale.

For the case of bottom grating structure at TM polarization illumination (Fig. 3(e)), one can observe additional enhanced absorbance features which cannot be attributed to guided modes. These do not vary considerably with alteration of the grating period, and are identified as local surface plasmon resonances, which exist at the interface between the metallic Ag and the dielectric Si layers. In Fig. 4 we show the normalized field distribution for the different modes, validating our conclusions as to the characteristics of the modes.

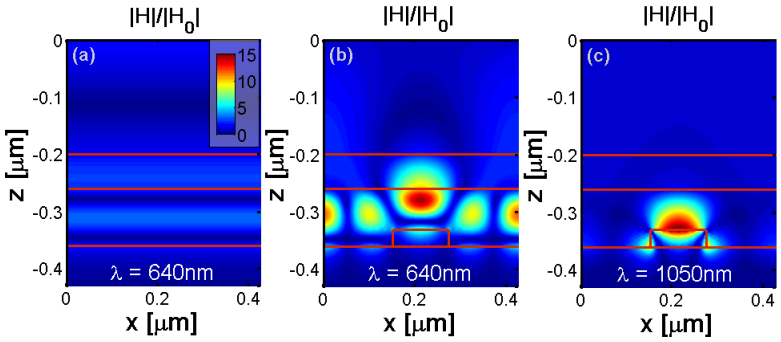

Fig. 4. Normalized and time averaged magnetic field intensity distribution for TM illumination for: (a) a bare solar cell with no grating structure, at 640nm wavelength; (b) bottom grating solar structure at 640nm wavelength; (c) bottom grating structure at 1050nm wavelength. The figures all appear in the same color scale. Plots (b) and (c) demonstrate strong light confinement in the presence of the grating structures, due to the coupling of the incident radiation to guided and localized modes, respectively. The grating parameters used for these plots are: grating period L = 425nm, grating height H = 30nm and grating width W = 110nm.

#181959 - $15.00 USD Received 18 Dec 2012; revised 13 Feb 2013; accepted 25 Mar 2013; published 9 Apr 2013

2.2 Dual-grating structures

We now turn to analyze the dual grating structure. Examining Figs. 2(c) and 2(d), we notice that the maximum current density occurs at a grating period of 425nm for both top and bottom single grating structures. Taking this fact into consideration, we find it reasonable to assume that a close to optimum result of the dual grating structure will also be obtained for a period of 425nm. Using this assumption we simplify the optimization procedure of the double grating cell, setting the period to a constant value of 425nm, and optimizing solely the width and height of the two gratings as well as the lateral shift between them. The optimized dual grating structure was attained for a top grating of H_t = 40, W_t = 80nm and of a bottom grating of H_b = 30, W_b = 110nm, with a relative lateral shift of S/L = 0.35 where S is the shift and L is the period. For such a structure the normalized current density enhancement is 1.86.

The dual grating structure exhibits similar absorption characteristics as the two single grating cells, as it couples light to the same basic photonic and plasmonic modes (Figs. 3(c) and 3(f)). To investigate the influence of lateral shift on the coupling of incident light to the modes supported by the structure, we present contour plots of absorption enhancement as a function of lateral shift and wavelength (Fig. 5). Basically, the structure supports the fundamental symmetric and anti symmetric modes (where the axis of symmetry is along the z axis) and their higher orders (higher Bloch modes). At TE illumination there is a clear mode splitting between the symmetric and the anti symmetric modes around wavelengths of 900 (1.4 eV, first Bloch mode) and 620nm (2.0 eV, second Bloch mode). At 900nm light couples to the fundamental guided TE_0 mode and has a periodicity of L (i.e. the fundamental Bloch mode). When the gratings are aligned with zero lateral shift (S/L = 0), the structure holds a mirror symmetry with respect to the z axis. Electric field is symmetric with regard to the symmetry axis of the grating unit cell and therefore light can only be coupled to symmetric modes. As the ratio S/L is increased, the symmetry of the structure is broken, and light can be coupled to anti symmetric modes as well [31]. For a Bloch mode of order m, when the two gratings are placed half a mode period away from each other ($m \cdot S/L = 0.5$), the structure returns to a symmetric state with respect to this mode. Therefore, the coupling of incident light to the anti symmetric mode of order m vanishes, and the dark anti symmetric mode is inaccessible once again. As an example, for the wavelength of 640nm, light couples to an anti symmetric second Bloch mode, and it therefore has a period of L/2. A mode of such periodicity is expected to disappear for quarter integer values of S/L, as indeed it appears in Fig. 5(a).

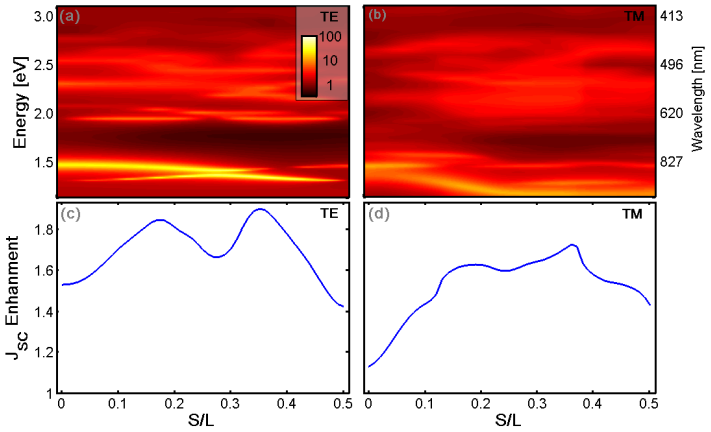

Fig. 5. Absorption enhancement as a function of wavelength and of the lateral shift between the two gratings for (a) TE and (b) TM polarized light, both at incident angle. Same color scale is used for both figures. (c) and (d) present the short circuit current density enhancement as a function of lateral shift for TE and TM, respectively.

#181959 - $15.00 USD Received 18 Dec 2012; revised 13 Feb 2013; accepted 25 Mar 2013; published 9 Apr 2013

Figure 5 shows additional effects which depend on the ratio S/L. As S/L is modified, both the width of the modes and their resonant frequencies are modified. These changes can be explained by the effect of mode interactions, which are affected by the relative shift between the two gratings [27, 28].

Note that the optimized structure above consists of two gratings which are spaced by a thin 10nm gap. However, this parameter is not crucial. For example, if we substantially increase the size of this gap to 30nm (by decreasing the height of the top grating), the current density J_{SC} enhancement would lose only 0.5% of current density enhancement.

Fabricated structures may deviate in their dimensions with respect to the optimal design. It is therefore valuable to examine the sensitivity of the design to small variations in the geometric parameters. Examining the sensitivity of the optimized dual grating structure, we found the tolerances of our design to be fairly relaxed. An error as large as 10nm in all heights and widths of the two gratings still result in J_{SC} enhancement of 1.6. Also worth mentioning is the fact that the height of the bottom grating is considerably more sensitive than other parameters. If the height of the bottom grating is held to good accuracy, the J_{SC} enhancement will reach a value of at least 1.8, even if we allow a large 10nm error in all other parameters.

So far the discussion was restricted to the case of normal incident angles. However, an additional important parameter of the proposed structure is its angular dependency. Figure 6 presents the current density enhancement as a function of the incident angle for both TE and TM polarizations. As expected, the current density is asymmetric with angle, since the structure design is asymmetric (S/L = 0.5). Observing Fig. 6 it can be seen that the dual grating design exhibits current enhancement for angles up to 40°. For angles up to ~15°, a significant enhancement of ~1.7-1.8 is observed. Since direct solar illumination is approximately 90% of global illumination and since the vast majority of daily illuminated solar energy (e.g. over 75% [39]) arrives around midday, at angles smaller than 40° – this information points to the significant advantage of the proposed dual grating design, compared to a bare solar cell.

Notice that the maximum current density enhancement is obtained at small angles of 3°-6°, and not at normal incidence as one would expect. This is explained as a result of our coarse optimization of the grating geometric parameters (for reasons of computational resources). Delicate stepping of all global parameters would result in maximum absorbance at normal incidence.

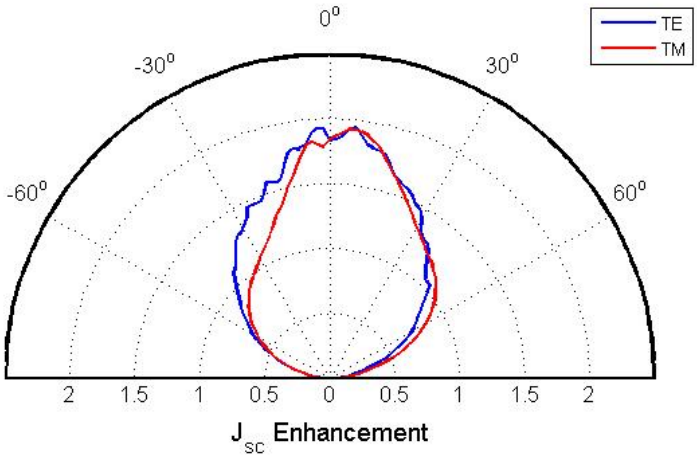

Fig. 6. Short circuit current density enhancement as a function of the incident angle for the optimized dual grating structure, under TE and TM polarized illumination.

#181959 - $15.00 USD Received 18 Dec 2012; revised 13 Feb 2013; accepted 25 Mar 2013; published 9 Apr 2013

Recently, a similar dual grating design was examined numerically in [23]. The structure examined there included a constant lateral shift of half a period between the top and bottom gratings (S/L = 0.5). Under AM1.5G the current density enhancement (compared to the same cell without any grating structures) of that structure is 1.176. However, varying the lateral shift S/L, we find that the cell could reach a current density enhancement of 1.194 with the proper optimized lateral shift of S/L = 0.39, as presented in Fig. 7. Furthermore, under half a period offset, the sensitivity of the current density enhancement to the exact relative position of the two gratings is much greater than for S/L = 0.39.

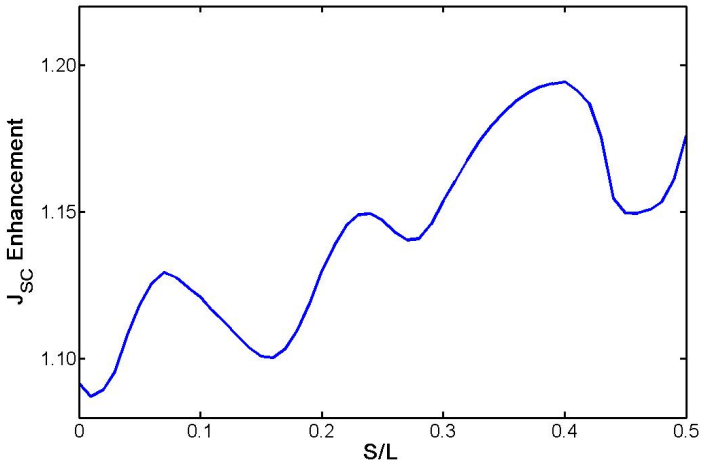

Fig. 7. Short circuit current density enhancement as a function of the relative lateral shift S/L for the grating structure of [23], under normal incidence. The maximum shift of 0.5 is determined by the symmetry of the structure. As shown, this shift is not optimal.

3. 2D dual grating structure

Further improvement in current density can be obtained by considering two dimensional grating structures. To validate this claim we present simulation results obtained for a dual grating structure with a top grating of H_t = 40nm $W_{t,x}$ = 80nm $W_{t,y}$ = 80nm, and a bottom grating of H_b = 30nm $W_{b,x}$ = 110nm $W_{b,y}$ = 110nm. These parameters are a direct extension of the optimized 1D grating to a square 2D grating, except for the height of the top grating (H_t) which was modified for practical reasons related to the numeric of computer simulation. Figure 8 shows the absorbance enhancement per wavelength and the current density enhancement of the 2D grating structure. As seen in Fig. 8(b), the total current density enhancement reaches a maximum of 2.15 for a grating wavenumber of 0.027nm^{-1} (periodicity of 234nm).

As mentioned above, these simulations were carried out using the FDTD algorithm, while the 1D gratings were simulated using the RCWA. These two codes were thoroughly compared for the case of a 1D grating structure and found to be in good agreement (~4% difference in overall absorption).

#181959 - $15.00 USD Received 18 Dec 2012; revised 13 Feb 2013; accepted 25 Mar 2013; published 9 Apr 2013

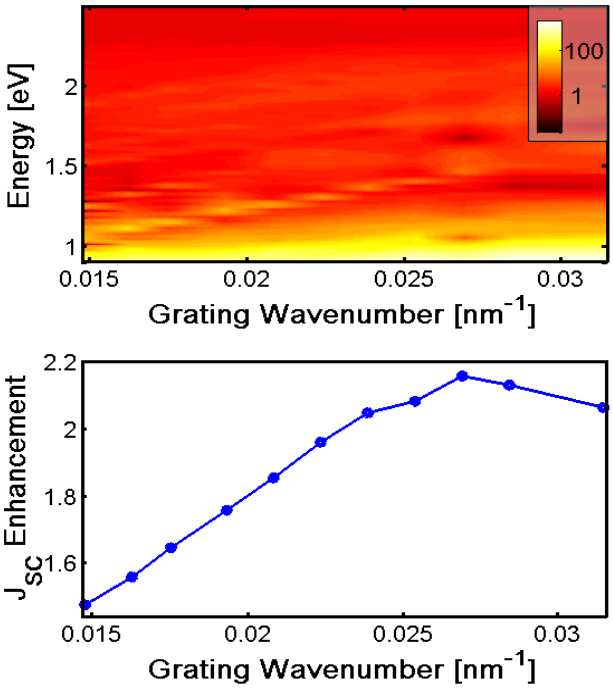

Fig. 8. 2D grating simulations under normal incidence. (a) Absorption enhancement as a function of wavelength and of grating wavenumber for the dual grating structure. The parameters of the dual grating structure examined are: top grating height of 30 nm, top grating duty cycles of 0.188, bottom grating height of 40 nm and bottom grating duty cycles of 0.259. (b) Integrated short circuit current density as a function of grating wavenumber for the same dual grating structure.

4. Conclusion

We have performed a detailed comparison between single and dual grating ultrathin plasmonic solar cells, and have found that the dual grating structure results in a substantial photocurrent enhancement, significantly higher than that obtained for each of the two single grating designs. Moreover, we demonstrated the importance of the relative shift between the two gratings – this parameter was shown to be crucial in enhancing the current density via the mechanism of coupling to dark modes providing additional absorption. Furthermore, we obtained improved efficiency over a broad range of incident angles. This is particularly important for low cost photovoltaic systems, with no sun tracking mechanisms.

While this paper is focused on the specific material system of silicon, the effect of incorporating two grating layers in plasmonic solar cells and controlling their relative position is quite general, and could be implemented in a wide variety of thin film solar cell designs. For instance, from fabrication and economic point of view it might very much be beneficial to use thin films of amorphous silicon as the active material, rather than silicon. A possible fabrication procedure of an amorphous silicon dual grating cell is described as follows. First, a layer of amorphous silicon is deposited on a sacrificial material, and is dopes to form a pn junction. Next, using lithography and etching techniques, the first grating structure is defined and metal is deposited to form an amorphous-silicon-metal grating. After creating the first grating, the structure is bonded to a substrate, and the sacrificial material is peeled off. Flipping the structure upside down, it is now possible to fabricate a second grating. Again, the grating is defined using lithography and etching techniques. Finally, ITO is deposited on the corrugated amorphous silicon layer, to form an amorphous-silicon-ITO grating.

#181959 - $15.00 USD Received 18 Dec 2012; revised 13 Feb 2013; accepted 25 Mar 2013; published 9 Apr 2013